Chapter

Resistance Welding of Aluminium Alloys with an Electromechanical Electrode Force System

Zygmunt Mikno

Abstract

The idea presented in this chapter is an innovative welding machine electrode force system. The operation, advantages of the new solution and the optimisation of the welding process were illustrated by the welding of aluminium bars (5182) (ø 4 mm). The solution involves controlling the force and/or displacement of welding machine electrodes. The modulation of electrode force significantly improves welding, particularly as regards aluminium alloys (requiring a very short welding process). The tests involved the numerical analysis of two electrode force systems, i.e. a conventional Pneumatic Force System (PFS) and an Electromechanical (Servomechanical Force) System (EFS). The numerical tests were performed using SORPAS software. FEM calculation results were verified experimentally. The technological welding tests were conducted using inverter welding machines (1 kHz) equipped with various electrode force systems. The research included metallographic and strength (peeling) tests and measurements of characteristic parameters. The welding process optimisation based on the EFS and the hybrid algorithm of force control resulted in i) more favourable space distribution of welding power, ii) energy concentration in the central weld zone, iii) favourable melting of the material within the entire weld transcrystallisation zone, iv) obtainment of the full weld nugget and v) longer weld nugget diameter.

Keywords: resistance welding of aluminium, electromechanical force system, cross-wire welding, projection welding, electrode force, FEM

1. Introduction

Force constitutes one of the most important parameters in the resistance welding process. The remaining parameters include current and current flow time. During cross-wire projection welding (particularly of aluminium alloys) involving the use of a conventional application, i.e. the pneumatic force system (PFS), it is very difficult, nearly impossible, to make a weld containing the full weld nugget. Aluminium, when subjected to welding, gets plasticised very quickly, which is responsible for the formation of the excessively large area of contact between welded elements and, consequently, results in a rapid decrease in current density. These are not favourable conditions for the melting of materials. In addition, the PFS is characterised by high inertia and the impossibility of performing fast changes

in force during current flow. For this reason, the value of preset force is usually constant and unfavourably too high. If the aforesaid force is excessively high, the high deformation of welded elements (bars) may occur as a result. The overly low force may lead to the formation of projection joint imperfections (such as expulsion caused by high temperature in contact areas) [1]. In the PFS, force applied during the welding process results from specific force preset by a pneumatic cylinder. The displacement of electrodes results from the action of this force and the changeable mechanical resistance of materials subjected to welding. A significant disadvantage of the above-presented method of control is the fact that neither force nor displacement (during the flow of current) is actually controlled.

An alternative solution requires another method making it possible to carry out faster changes in force during the welding of materials [1–3]. In publication [1], the authors emphasise the growing popularity of the electromechanical (servomechanical) force system (EFS) and an advantage consisting in an increase in an electrode displacement rate during welding. In publication [2] the authors inform about the possible extension of the window of technological parameters, improving the weldability of materials. In work [3, 4] the authors mention the possible modulation of force and its fast changes, particularly at the final stage of the welding process. The authors stress an increase in electrode service life in spot resistance welding and the application of servomotors in the riveting technology [5]. In publications [3, 6] authors state that the EFS has eliminated the dynamic impact of electrodes against a welded material (during the exertion of initial force), which was characteristic of pneumatic actuators. The EFS has enabled a gentle "touch" of an electrode against a material being welded. In work [3] the authors enumerate other advantages of the EFS including (i) superior (faster) operation of a welding gun (servo) in space, (ii) greater repeatability of force, (iii) reduced noise, (iv) shorter welding time and (v) shorter movement during the closing and opening of the electrodes, extending the service life of related mechanisms.

The tests discussed in the article aimed at replacing the PFS with the EFS. It was also important to appropriately control the servomotor in order to perform the controlled movement/shift of electrodes, particularly during the flow of current. The control process has changed considerably, i.e. the displacement of electrodes is a preset parameter and resultant force depends on the displacement of electrodes and the resistance of the deformation of a contact area being heated. Available reference publications do not contain information about such a method of electrode movement control as that presented in this study.

The authors [7, 8] describe a new control system and the results of its operation, particularly noticeable in projection welding. In [7, 9] the authors refer to a new control system applied when welding sheets with an embossed projection. Another use of the new solution, i.e. cross-wire welding, and the welding of nuts are presented in publications [10–12] respectively.

In publications [7–12] the authors present a completely different solution, i.e. the slowing down of the displacement of an electrode during the projection welding of sheets with an embossed projection. This approach is new and characterised by advantages which are definitely worth mentioning. The above-named idea can be used in relation to aluminium alloys as these materials require a very short welding time (50 ms). It is possible to decrease the penetration of bars and to generate more energy in the optimum place, i.e. in the contact area between the bars. The new idea of electrode displacement control significantly alters the previous approach to the course of the resistance welding process (projection cross-wire welding) and considerably influences the development of the entire research area (pressure welding).

2. Characteristics of welding machine electrode force systems (EFS and PFS)

The essence of the EFS (in comparison with that of the PFS) involves a significantly higher rate of changes, i.e. changes in the force and/or displacement of electrodes. During the resistance welding process, the aforesaid approach is of significant importance because of the fact that the time of welding current flow in typical applications is very short and amounts to 0.2 s (200 ms). The optimisation (improvement) of the welding technology requires the modulation (change) of electrode force during the above-named time. Regrettably, as regards the conventional electrode force system (PFS), common in industrial applications, such modulation is impossible because of the significant inertia (delay) of this solution. **Figure 1** presents exemplary courses of electrode force and displacement in relation to the PFS (dashed line) and EFS (full line). The aforesaid courses refer to two operating modes, i.e. the approach mode and the force mode. The time necessary to obtain previously adjusted electrode force, i.e. electrode force stabilisation time (EFST), by the PFS exceeds 200 ms. The EFST parameter related to the EFS is significantly shorter and restricted within the range of 50–80 ms, depending on the configuration of the EFS (servomotor power, gear etc.). An important characteristic of this solution is the possibility of modulating the course of electrode force during the flow of current, which is nearly impossible as regards the PFS.

The EFS can be controlled in two different manners, i.e. using an algorithm enabling the control of force and an algorithm enabling the control of the (electrode) displacement rate. The first of the algorithms is already used in industrial practice. The time of delay in the stabilisation of preset electrode force is restricted within the range of 50–80 ms. In such an operating mode, it is possible to modulate force and obtain two or three different values (in CFT amounting to 200 ms).

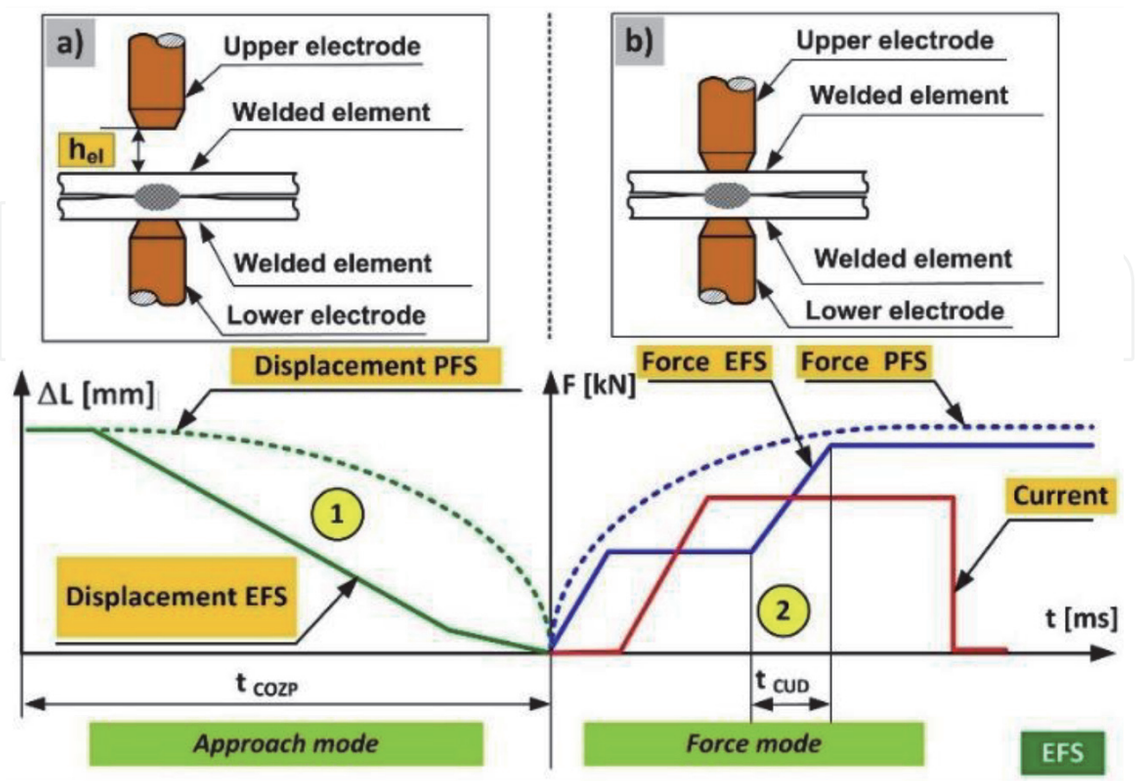

Figure 1.
Comparison of the EFS and PFS based on exemplary courses of electrode force and displacement in relation to operating modes: (a) approach mode and (b) force mode [13].

The aforesaid time (50–80 ms) depends on the configuration of the EFS (motor, gear) and on the preset value of force. In turn, the second algorithm (developed by the author) has been used to weld demanding (in the aforesaid respect) materials, i.e. aluminium alloys. Until today, the author has not come across any information concerning the method of control presented in this chapter.

The unique characteristic of the EFS and of the solution is a special algorithm, where the control of the displacement of electrodes results in the exertion of electrode force. In the above-named algorithm of control, delays between preset and actual values are counted in milliseconds, making it possible to develop a very fast algorithm enabling the exertion of variable (electrode) force [9]. The above-presented manner of controlling the force of electrodes through the control of their displacement alters previous views on methods enabling the control of force (movement of electrodes) in the resistance welding process.

3. Methodology of numerical and experimental tests

The crosswise projection welding of aluminium bars (Al 5182) performed using the PFS was subjected to numerical analysis verified experimentally and aimed to subsequently optimise the welding process performed using the EFS system. The assumed acceptance criteria included (i) obtainment of the full weld nugget having a diameter of not less than 1.5 mm, (ii) lack of deformation and the penetration of the bars less than 20% of the diameters of elements subjected to welding (Δl_{PP} = 1.6 mm), (iii) lack of overheating in the area of contact between the electrode and the material being welded ($T_{e\text{-}m\ max} \leq 500°C$), (iv) lack of expulsion and (v) maximum current flow time $t_{PP\ max}$ = 63 ms. An additionally expected result was the reduction of (welding) current flow time.

The material of bars subjected to welding and adopted in FEM-based calculations was aluminium alloy grade 5182 with solidus (temperature) being 577°C and liquidus amounting to 638°C [14]. The chemical composition of the aluminium alloy grade Al 5182 used in the bars is presented in **Table 1**.

3.1 FEM calculations

The numerical calculations were performed using the SORPAS® 3D software program [15]. The calculations were carried out for ¼ of the model and its mirror reflection in relation to the plane determined by x-z-axes and y-z-axes (**Figure 2**). The mesh in the area of contact between the elements (bars) subjected to welding was concentrated in order to provide the appropriate accuracy of calculations. The lack of proper mesh density resulted in the lack of contact between the elements subjected to welding and, consequently, incorrect calculations.

3.2 Numerical (FEM) model

The numerical model of the crosswise welding of bars is presented in **Figure 2**. The calculations were performed using the 3D model [15].

Al (max)	Mn (max)	Mg (max)
95.2	0.35	4.5

Table 1.
Chemical composition of the materials subjected to welding, i.e. bars made of aluminium alloy grade Al 5182.

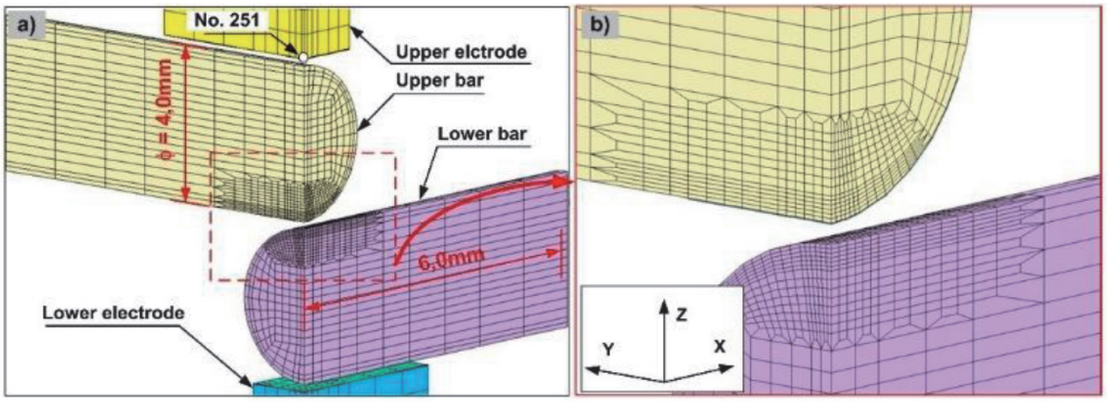

Figure 2.
Model (3D) of the crosswise welding of aluminium bars (Al 5182).

The numerical calculations included the analysis of (i) waveforms of dynamic resistance and momentary power, (ii) energy supplied to the weld, (iii) diameter and volume of the molten material of the weld nugget, (iv) displacement of electrodes (penetration of bars), (v) expulsion (if any) and (vi) temperature in the electrode bar contact area (Te-m, point 251—**Figure 2a**). The primary objective included the determination of the most favourable space distribution of welding power enabling the melting of the material in the central zone of the joint (to obtain the full weld nugget). As in all other cases of projection welding, the aspect of particular importance was the beginning of the welding process, i.e. the beginning of welding current flow.

3.3 Process parameters

The assumptions adopted in the numerical model included (i) copper electrodes (A2/2) and (ii) elements subjected to welding, i.e. aluminium (grade Al 5182) bars having a diameter of 4 mm and a length of 12 mm (**Figure 2a**). The 3D model was composed of approximately 9000 elements. To ensure the required accuracy of calculations, it was necessary to concentrate the mesh in the area of contact between the bars (**Figure 2b**).

Data related to the electrodes and materials subjected to welding and used in the FEM calculations were obtained from the SORPAS software program database (**Table 2**) [14]:

- Aluminium bars Al 5182—material database designation SORPAS AA5182(O): Al95, Mn0.25, Mg4.5, solidus (577°C), liquidus (638°C) (**Table 3**)

- Electrodes of class A2/2 CuCrZr (**Table 4**)

Based on the present recommendations and guidelines concerning the crosswise projection welding of bars, the following ranges of parameters were adopted for:

- PFS [16–18]: (i) welding current I = 8.0–12.0 kA, (ii) welding current flow time t_{PP} = 3 ms (upslope) + 60 ms (primary welding time) and (iii) electrode force F = 0.5–1.5 kN

- EFS: (i) welding current I = 8.0 kA, (ii) welding current flow time t_{PP} = 3 ms (upslope) + 35 ms and (iii) control of electrode displacement during the flow of welding current [11].

Time step increment	Squeeze	Upslope	Weld	Hold	Unit
Pneumatic force system	500	10–70	200	500	ms
Electromechanical force system	200	10	250–300	500	ms
Time step	0.1	0.1	0.1	1	ms
Convergence control					
	Convergence accuracy				
Electrical model	1.00E−5				
Thermal model	1.00E−5				
Mechanical model	1.00E−5				
Welding parameters					
Welding current	DC				
Heat loss to the environment					
Air temperature	20			°C	
Heat transfer rate	300			$W/m^2 K$	
Electrode dimensions					
Length × width	10.0 × 8.0			mm	
Electrode height	5			mm	
Contact between welded elements	Sliding				

Table 2.
Parameters of the SORPAS software program used in numerical (FEM) calculations.

The numerical calculations were performed in relation to a DC inverter welding machine (1 kHz). The remaining welding cycle parameters are presented in **Table 2**. **Table 5** presents the preset parameters of the welding cycle and the parameters characteristic of variants selected for FEM calculations.

The PFS variants are designated as P1 ÷ P9 (P, pneumatic system), whereas the EFS variants are designated as E1 ÷ E3 (E, electromechanical system). The analysis of the welding process performed in relation to the PFS aimed to investigate and depict the variability of process parameters and determine the most favourable welding conditions (MFWC). The results of the analysis revealed the lack of the monotonicity of the weld nugget growth (**Figure 4a**) visible in relation to a force of 0.75 kN. For this reason it was necessary to perform additional calculations in this area, i.e. for a value of 0.7 kN and that of 0.8 kN. In total, the analysis of the process was focused on 35 points (I = 8/9/10/11/12 kA, F = 1.5/1.25/1.0/0.8/0.75/0.7/0.5 kN).

The numerical optimisation concerning the process involving the use of the EFS was performed for lower values of current than those analysed in relation to the PFS (8.0 ÷ 10.0 kA). The numerical calculations were continued until the occurrence of one (of six) previously adopted boundary conditions.

3.4 Experimental tests

The experimental tests were performed using inverter welding stations (DC 1 kHz) shown in **Figure 3a** (PFS) and **Figure 3b** (EFS). The welding parameters were recorded using a LogWeld 4 measurement device.

The results obtained in the numerical calculations were verified experimentally. The experimental tests involved nine variants (P1–P9) from **Table 5** (PFS). All of the variants (**Figure 6**) were subjected to destructive tests (peeling), confirming the

Temperature (°C)	Thermal conductivity (W/m·K)	Temperature (°C)	Heat capacity (J/kg·K)	Temperature (°C)	Resistivity (mΩ·m)	Temperature (°C)	Mass density (kg/m^3)	Temperature (°C)	Thermal expansion coefficient ($10^{-6}/^{O}C$)	Temperature (°C)	Young's modulus of elasticity (kN/mm^2)
25	123.0	23	794	25	0.056	25	2660	25	23.9	25	70.0
100	134.0	50	825	100	0.068			250	25.0		
200	147.6			200	0.079						
400	160.9			400	0.103						
500	164.3			500	0.115						
600	163.3			600	0.131						

Table 3.
Material parameters of welded materials (bars Al 95 Mn0.25, Mg4.5) [14].

Temperature (°C)	Thermal conductivity (W/m·K)	Temperature (°C)	Heat capacity (J/kg·K)	Temperature (°C)	Resistivity (mΩ·m)	Temperature (°C)	Mass density (kg/m^3)	Temperature (°C)	Thermal expansion coefficient ($10^{-6}/^{O}C$)	Temperature (°C)	Young's modulus of elasticity (kN/mm^2)
20	326.6	20	372	20	0.022	20	8890	25	16.5	25	117.0
100	342.1	127	402	100	0.027	1080	8320				
300	338.0	327	422	200	0.038						
500	340.3	527	438	300	0.042						
700	332.0	727	456	400	0.049						
900	321.8	927	485	500	0.057						
				600	0.065						
				700	0.073						
				800	0.082						
				900	0.091						
				1000	0.102						
				1100	0.220						

Table 4.
Material parameters of electrodes ISO 5182 A2–2 electrode CuCrZr [14].

No.	Variant	Current	Welding time	Force	Penetration Δ l	Weld diameter	Weld volume	Energy	Remarks
		kA	ms	kN	mm		mm^3	kJ	
1		2	3	4	5	6	7	8	9
Pneumatic system (PFS)									
1	P1	8.0	63	1.5	1.47	0.1	0.0	0.17	Overly small weld nugget diameter
2	P2	10.0	46		2.38	0.1	0.0	0.17	Excessive penetration of bars
3	P3	12.0	29		1.85	0.0	0.0	0.15	
4	P4	8.0	63	1.0	1.00	0.2	0.0	0.20	Overly small weld nugget diameter
5	P5	10.0	59		2.13	1.5	0.9	0.23	Most favourable welding conditions in spite of significant penetration of bars
6	P6	12.0	46		2.54	0.2	0.0	0.30	Overly small weld nugget diameter
7	P7	8.0	63	0.5	0.57	0.3	0.1	0.25	Overly small weld nugget diameter
8	P8	10.0	8		0.19	1.5	0.7	0.07	Unfavourably short welding time, high dynamics of the force system required
9	P9	12.0	5		0.15	0.8	0.1	0.05	Overly small weld nugget diameter
Electromechanical (servo) system (EFS)									
10	E1	8.0	38	Servo force	0.6	1.95	4.5	0.16	OK, full weld nugget, nugget diameter > 1.6 mm, penetration of bars <1.6 mm
11	E2	9.0	25		1.2	2.00	5.3	0.10	
12	E3	10.0	20		1.5	2.20	5.6	0.13	

Red colour, unacceptable param.; green colour, acceptable param.; orange colour, the most favourable welding conditions.

Table 5.
Preset welding cycle parameters and parameters characteristic of selected variants in the FEM calculations related to the PFS and EFS (FEM).

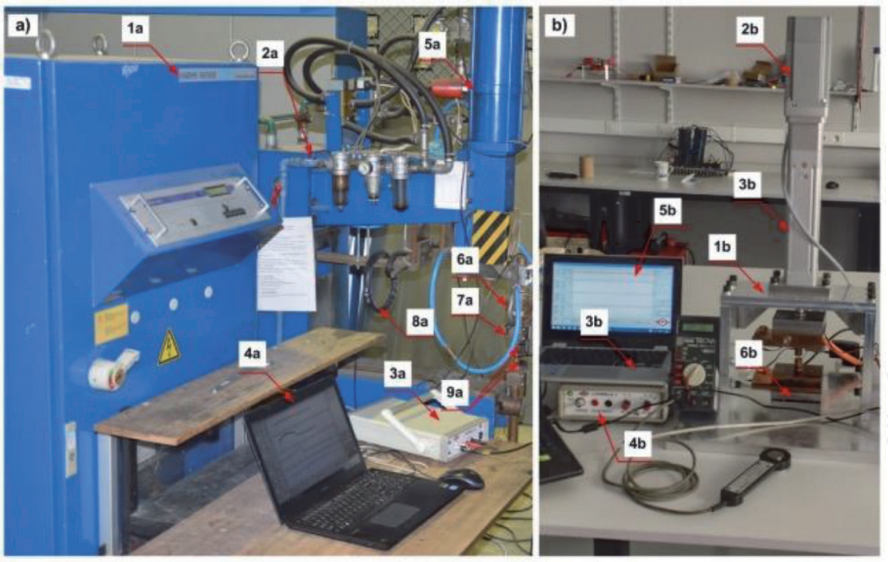

Figure 3.
Welding machine stations: (a) SPD: (1a) inverter welding power source Harms & Wende (25 kA, 1 kHz), (2a) welding machine housing ASPA (5.5 kN), (3a, 4a) measurement device LogWeld 4, (5a) pneumatic actuator, (6a) head for measurements of electrode force, (7a) laser sensor for displacement measurements, (8a) welding current measurement sensor and (9a) leads for measurements of welding voltage. (b) SED: (1b) electromechanical welding machine F = 2 kN, (2b) servomotor, (3b) linear gear, (4b, 5b) measurement device LogWeld 4 and (6b) electrode force measurement module.

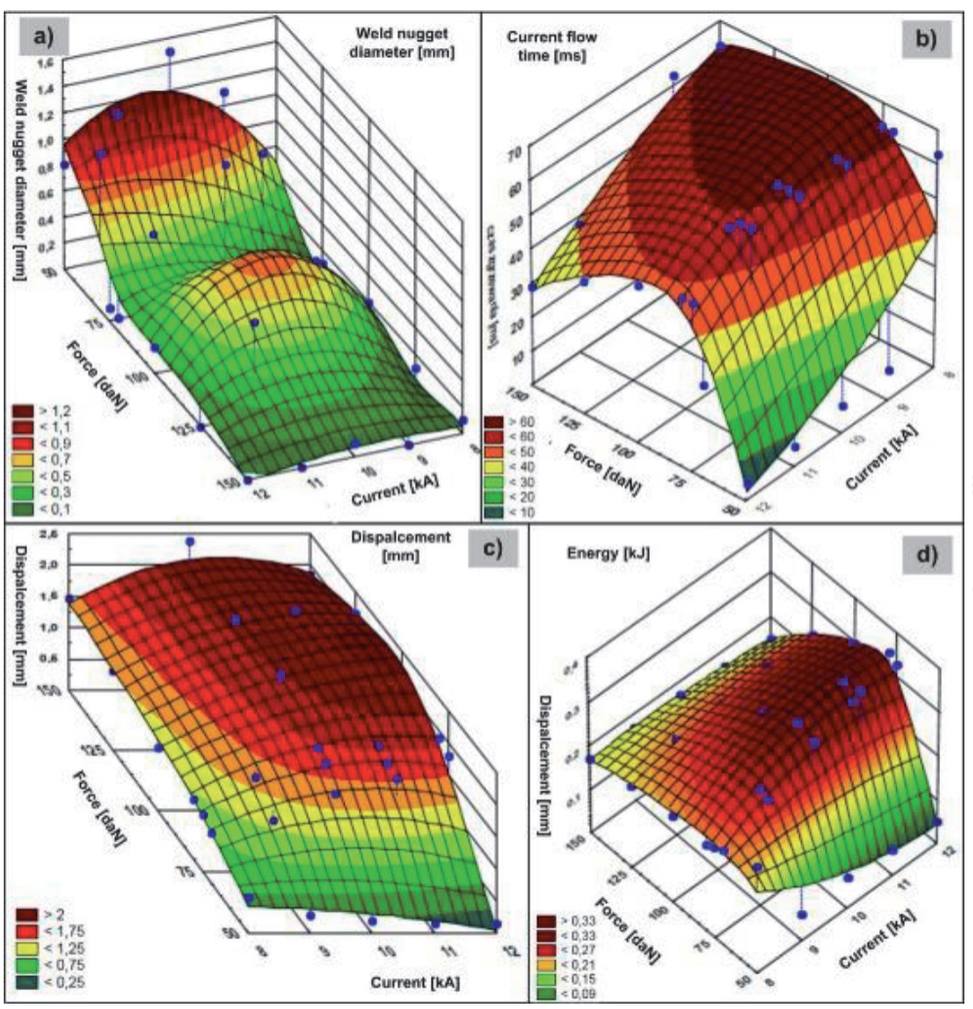

Figure 4.
Variability of characteristic parameters in relation to the PFS (Al 5182, ϕ = 4 mm, MES) [11]: (a) weld nugget diameter, (b) current flow time, (c) displacement (of electrodes - penetration of bars), (d) energy (of welding).

formation of the ring weld. However, none of the PFS variants satisfied the previously assumed criteria. Nonetheless, in spite of the exceeding of the previously assumed value of bar penetration and the obtainment of the ring weld, variant P5 was adopted as the reference variant for further optimisation-related activities. The reason for such a choice resulted from the fact that the aforesaid variant (P5) enabled the obtainment of the longest weld nugget diameter. Parameters similar to those used with reference to variant P5 were used in additional technological welding tests (**Table 6**, PE1–PE3). The results related to the preset parameters of the technological cycle and characteristic parameters of selected welding tests involving the use of the PFS and variants PE1–PE3 are presented in **Table 6**.

The welding cycle parameters used in relation to variants PE1–PE3 included electrode force F = 1.0 kN, welding current I = 9.0–10 kA and welding time t_{PP} = 43–63 ms. The metallographic tests involving the above-named variants confirmed the results obtained in the numerical calculations, e.g. the ring-like shape of the weld nugget.

Key: I_{rms}, root-mean-square current; PE, pneumatic experiment.

4. Process optimisation

The optimisation of the crosswise projection welding of bars was performed using the EFS. The primary criterion of the optimisation process involved the obtainment of the full weld nugget having a diameter of not less than 1.5 mm. The optimisation process assumed the use of the EFS and, in addition, the adjustment of the lowest possible value of welding current.

The optimisation process also aimed to adjust appropriate and lower electrode force than that applied initially in the process performed using the PFS and to control the displacement of the electrodes so that it could be possible to obtain the most favourable space distribution of welding power, i.e. ensuring the emission of appropriately more heat (energy) in the central part of the contact area between elements being welded (in order to melt the material of these elements) [10, 11].

The preset welding cycle parameters (grey) and the parameters characteristic of the technological welding tests performed using the EFS are presented in **Table 7**. The technological welding tests were performed using a current of approximately 8.0 kA, i.e. the lowest value analysed in relation to the welding process performed using the PFS. The aforesaid value of current applied in the PFS, within the entire range of analysed values of electrode force (0.5 kN ÷ 1.5 kN), was insufficient to melt the material of the elements subjected to welding. The welding process was optimised using the EFS and a welding current of 8.0 kA and that of 8.5 kA as well as the appropriate profile of electrode force (variants EE1 and EE2, **Table 7**).

5. Results

5.1 FEM calculation results

The PFS-related numerical calculation results are presented in **Figure 4** and **Table 8**. The results are presented in spatial diagrams developed using the Statistica software program [19]. **Figure 4** presents (in the form of a spatial diagram) the formation of the weld nugget diameter (**Figure 4a**), welding time (**Figure 4b**), bar

No.	Variant no.	Preset parameters					Recorded parameters				
		Electrode force	Upslope		Main welding time		Total current (I_{rms})	Welding energy	Bar penetration (displacement of electrode)	Weld diameter	Number of tests
			Current	Time	Current	Time					
		kN	kA	ms	kA	ms	kA	kJ	mm	mm	pcs
		A	B1	B2	C1	C2	D	E	F	G	H
1	PE1	1.0	10.0	3	10.0	40–60	10.0	0.23	1.50	1.5	20
2	PE2	1.0	9.5	3	9.5	50–70	9.5	0.21	1.38	1.3	20

Table 6.
Preset and characteristic parameters of the PFS (experiment) [11].

No.	Variant no.	Preset parameters											Recorded parameters			
		Force			Upslope		Main welding time		Total current (I_{rms})	Electrode displacement and time				Welding energy	Bar penetration (displacement of electrode)	Weld diameter	Number of tests
		Initial	Min.	Max.	Cur	Time	Cur.	Time		$t_1/\Delta l_1$	$t_2/\Delta l_2$	$t_3/\Delta l_3$	$t_4/\Delta l_4$				
		kN			kA	ms	kA	ms	kA	ms/mm				kJ	mm	mm	pcs
		A1	A2	A3	B1	B2	C1	C2	D	E0	E1	E2	E3	F	G	H	I
1	EE1	1.0	0.4	1.0	8.0	3	8.0	45	8.0	10 0.08	30 0.25	10 0.05	30 0.25	0.16	0.70	1.87	20
2	EE2	1.0	0.4	1.0	8.5	3	8.5	40	8.5	10 0.08	25 0.25	7 0.05	30 0.25	0.20	0.75	1.92	20

Key: I_{rms}, root-mean-square current; EE, electromechanical experiment.

Table 7.
Preset and characteristic parameters of the EFS (experiment) [11].

penetration depth (electrode displacement) (**Figure 4c**) and welding energy (**Figure 4d**). The correlations are presented in relation to various values of welding current and electrode force.

Numerical values related to the graphic representation of the results presented in **Figure 4** are presented in **Table 8(a-d)**, containing, in addition, information about the following:

- Unsatisfied criterion (**Table 8e**), i.e.:
- $t_{PP\ max}$—maximum time of welding current flow ($t_{PP\ max}$ = 63 ms)
- ΔL—displacement of electrodes (penetration of bars, ΔL_{max} = 1.6 mm, 20% of the diameters of the bars)
- W—expulsion
- Weld itself (**Table 8f**), i.e.:
- D—weld nugget diameter: below 0.7 mm; (*S*, *small nugget diameter*)
- R—ring-shaped weld nugget: 0.7 mm < D ≤ 1.5 mm; (*R*, *ring weld nugget*)
- F—full weld nugget: D > 1.5 mm; (*F*, *full weld nugget*)
- Weld nugget volume (**Table 8g**)

    a. current flow time

    b. displacement (of electrodes - penetration of bars)

    c. welding energy.

The results presented in **Table 8** supplement the information concerning the (course of) variability of the characteristic parameters from **Figure 4**.

Table 8 also contains the numerical calculation results obtained for the EFS (green). In relation to all of the previously assumed parameters, the conditions concerning the optimised method of control were satisfied.

The comparison of the FEM calculation results (in the form of the distribution of temperature) related to the two (i.e. PFS and EFS) electrode force systems, different values of welding current (8.0 and 10.0 kA) and various ranges of temperature (20–638°C and 577–638°C) is presented in **Figure 5**.

5.2 Experimental test results

The PFS-related technological welding tests involving the aluminium bars were performed in relation to all of the nine variants P1–P9 from **Table 5**. The results after the peeling tests are presented in **Figure 6**.

Parameters similar to those used with reference to variant P5, i.e. in relation to which the longest weld nugget diameter was obtained, were used in additional technological welding tests performed in relation to a wider welding current range of 9.0–10.0 kA. Results (in the form of metallographic structures) related to the above-presented parameters are presented in **Figure 7**. The preset

Current [kA]	(a) Weld nugget diameter [mm]							
	0.5 mm < d < 1.5 mm				d < 0.5 mm			Servo
	Force [kN]							
	1.50	1.25	1.00	0.80	0.75	0.70	0.50	
8	0.1	0.1	0.2	0.0	0.1	0.0	0.3	1.95
9	0.0	0.0	0.6	0.0	0.0	0.0	1.1	2.00
10	0.1	0.1	1.5	1.1	0.1	0.0	1.5	2.20
11	0.0	0.7	0.3	0.0	0.2	0.5	1.1	
12	0.0	0.0	0.2	0.1	0.1	1.2	0.8	
Current [kA]	**(b) Current flow time [ms]**							
	t_weld >63 ms				t_weld <63 ms			Servo
	Force [kN]							
	1.50	1.25	1.00	0.80	0.75	0.70	0.50	
8	63	63	63	63	63	63	63	38
9	63	63	63	63	63	63	9	25
10	46	56	59	63	63	63	8	20
11	38	48	53	60	63	63	6	
12	29	39	46	49	49	27	5	
Current [kA]	**(c) Final electrode displacement [mm]**							
	D < 1.6 mm				D > 1.6 mm			Servo
	Force [kN]							
	1.50	1.25	1.00	0.80	0.75	0.70	0.50	
8	1.47	1.25	1.00	0.95	0.9	0.80	0.57	0.60
9	1.60	1.62	1.50	1.30	1.10	1.00	0.28	1.20
10	2.38	2.07	2.13	1.75	1.70	1.40	0.19	1.50
11	2.00	2.20	1.90	1.80	1.70	1.65	0.16	
12	1.85	2.15	2.54	1.90	0.80	0.70	0.15	
Current [kA]	**(d) Energy [kJ]**							
	E < 0.16		0.16 < E < 0.32			E ≥ 0.32		Servo
	Force [kN]							
	1.50	1.25	1.00	0.80	0.75	0.70	0.50	
8	0.17	0.19	0.20	0.20	0.21	0.22	0.25	0.16
9	0.17	0.22	0.25	0.27	0.27	0.26	0.06	0.10
10	0.17	0.23	0.29	0.33	0.29	0.32	0.07	0.13
11	0.16	0.24	0.30	0.35	0.32	0.36	0.06	
12	0.15	0.24	0.30	0.34	0.33	0.22	0.05	
Current [kA]	**(e) Achieved criterion**							
	D > 1.6 mm		t, welding time (63 ms)			E, expulsion		Servo
	Force [kN]							
	1.50	1.25	1.00	0.80	0.75	0.70	0.50	
8	t	t	t	t	t	t	t	OK

Current [kA]	**(e) Achieved criterion**							
	D > 1.6 mm		**t, welding time (63 ms)**			**E, expulsion**		**Servo**
	Force [kN]							
9	t	t	t	t	t	t	E	OK
10	D	D	D	t	t	t	E	OK
11	D	D	D	P	t	t	E	
12	D	D	D	D	D	E	E	
Current [kA]	**(f) Type of nugget**							
	F, full nugget		**R, ring nugget**			**L, low nugget (f < 0.7 mm)**		**Servo**
	Force [kN]							
	1.50	1.25	1.00	0.80	0.75	0.70	0.50	
8	L	L	L	L	L	L	L	F
9	L	L	L	L	L	L	R	F
10	L	L	R	R	L	L	R	F
11	L	L	L	L	L	L	R	
12	L	L	L	L	L	R	R	
Current [kA]	**(g) Weld nugget volume [mm^3]**							
	0.5 mm < V (vol.) < 1.5 mm^3				**V (vol.) < 0.5 mm^3**			**Servo**
	Force [kN]							
	1.50	1.25	1.00	0.80	0.75	0.70	0.50	
8	0.0	0.0	0.0	0.0	0.0	0.0	0.1	4.50
9	0.0	0.0	0.0	0.0	0.0	0.0	0.2	5.25
10	0.0	0.0	0.9	0.3	0.0	0.0	0.7	5.60
11	0.0	0.2	0.0	0.0	0.0	0.2	0.5	
12	0.0	0.0	0.0	0.0	0.0	1.3	0.1	

Table 8.
FEM calculation results concerning the crosswise projection welding of bars in relation to the PFS and EFS (AL 5182) [11].

welding cycle parameters in relation to variants PE1 and PE3 are presented in **Table 6**.

In terms of the EFS, the technological welding tests were performed in relation to a current of 8.0 kA and that of 8.5 kA (**Table 7**, variants EE1 and EE2). The comparative results in the form of the metallographic structures of the joints are presented in **Figure 8a1–a2** and **b1–b2** (in relation to the PFS and EFS, respectively).

6. Discussion

6.1 FEM calculations

The PFS-related conclusions based on the analysis of the results presented in **Figure 4** and **Table 8** are the following:

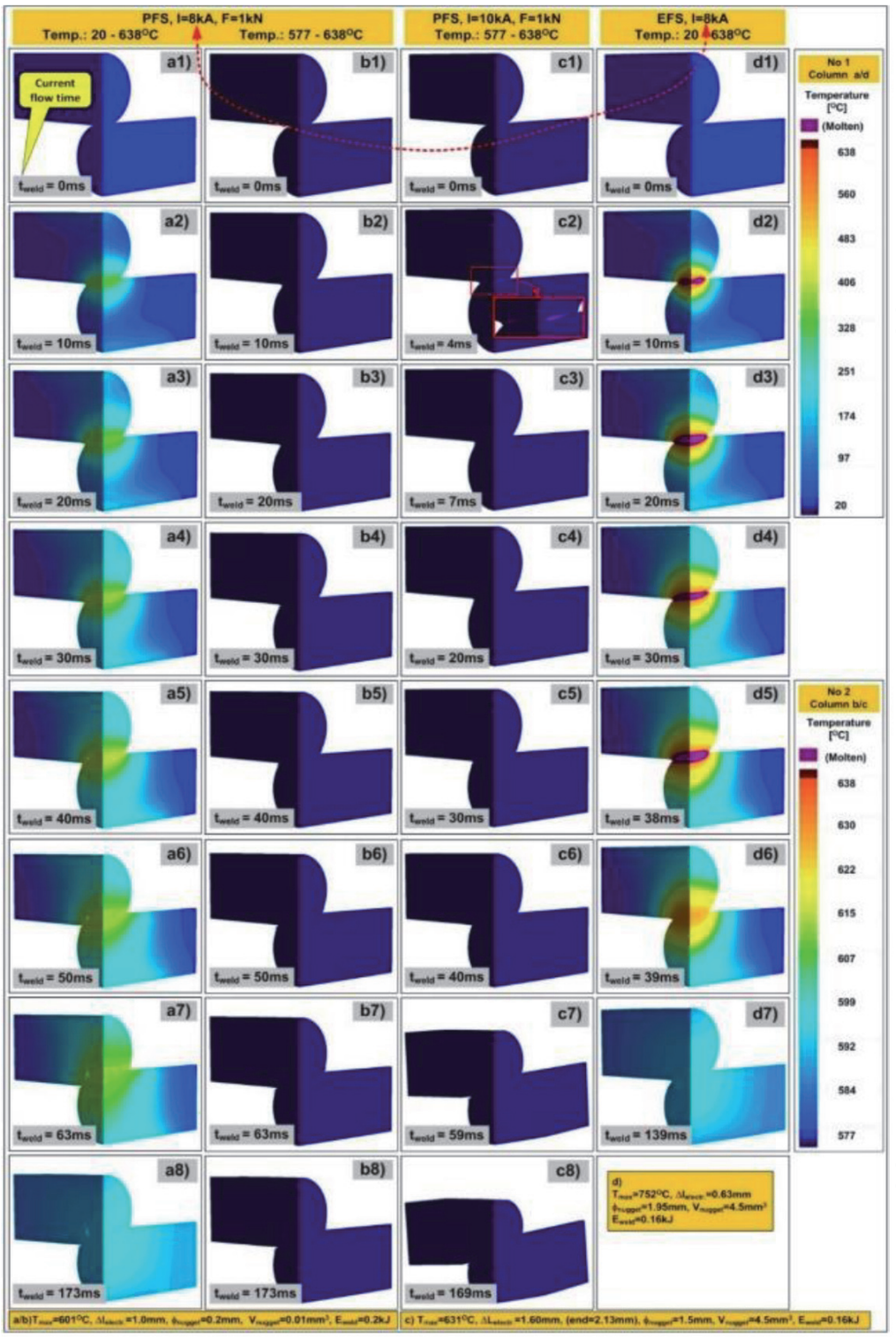

Figure 5.
Distribution of temperature in the welding area (FEM) in relation to: (a/b) PFS (I = 8 kA, F = 1.0 kN), (c) PFS (I = 10 kA, F = 1.0 kN) and (d) EFS (I = 8.0 kA, force exerted by the servomotor).

- Maximum obtainable weld nugget diameter amounted to 1.5 mm (**Table 8a**, parameter field 1).

- Ring-shaped weld was formed (**Table 8f**, parameter field 2) within the entire range of the variability of welding current parameters and that of electrode force, also as regards the longest obtained weld nugget diameter (i.e. restricted within the range of 1.0–1.5 mm).

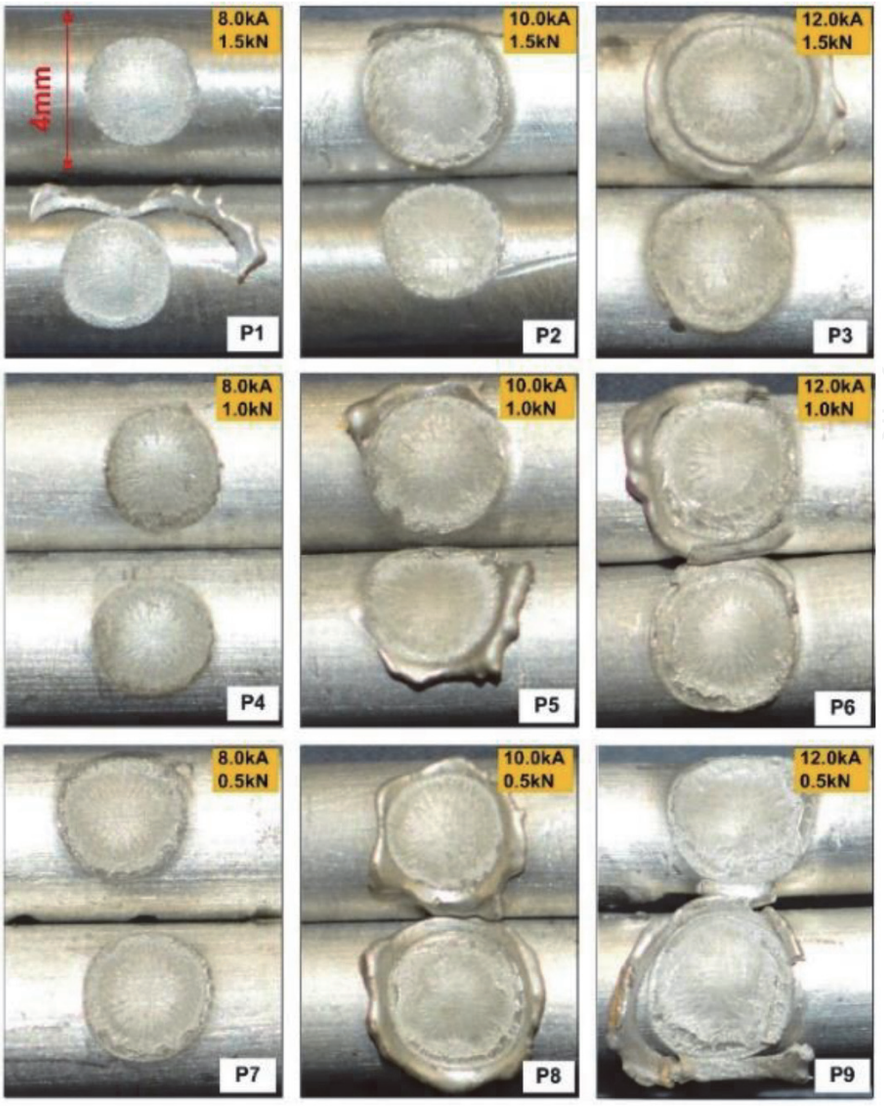

Figure 6.
Specimens after the peeling tests (PFS, variants P1–P9).

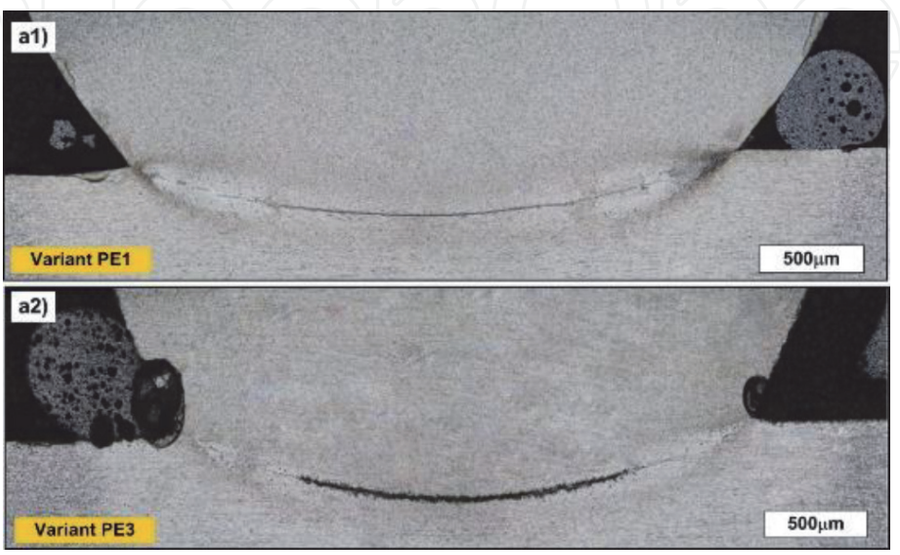

Figure 7.
Results of the metallographic tests for the PFS (F = 1 kN, I = 9.0/10.0 kA).

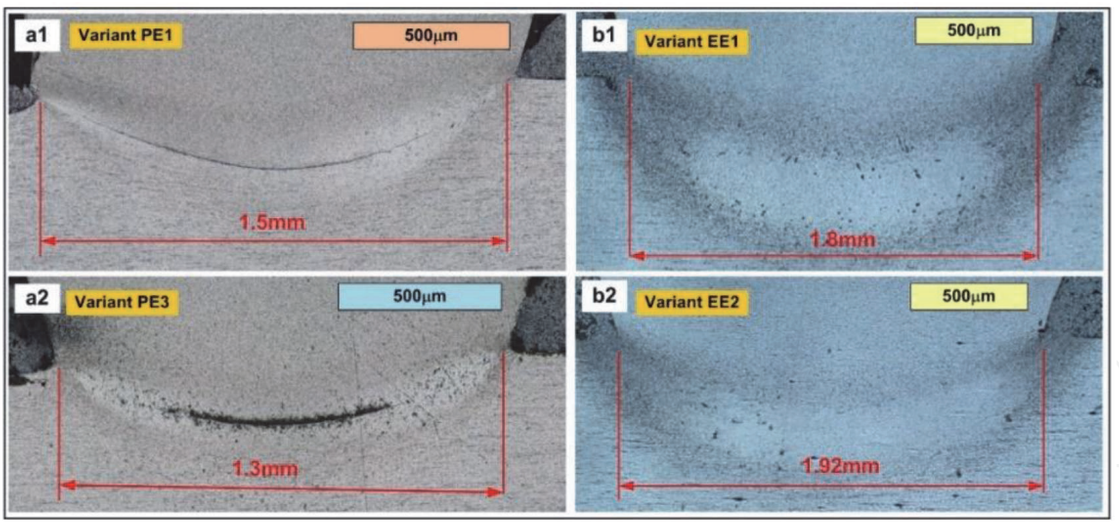

Figure 8.
Metallographic test results in relation to [11]: (a) PFS, (a1) variant PE1 and (a2) variant PE3; (b) EFS, (b1) variant EE1 and (b2) variant EE2.

- Criterion concerned with the exceeding of the maximum welding current flow time ($t_{PP\ max}$ = 63 ms) was observed in relation to the lower value of welding current (**Table 8e**, parameter fields 3a and 3b, respectively).

- The highest volume of the molten material was observed in relation to the highest values of welding current and the lowest values of electrode force (**Table 8g**, parameter field 4). The above-named parameters were also connected with relatively low welding energy (**Table 8d**, parameter field 5). However, welding time was relatively short and amounted to a few milliseconds. In the aforesaid case, even the slight exceeding of the welding time resulted in expulsion (**Table 8e**, parameter field 7).

- Excessive penetration of the bars (above the acceptable value) was related to the obtainment of the higher value of welding current and the higher value of electrode force (**Table 8c**, parameter field 6a (final penetration), and **Table 8e**, parameter field 6b (penetration value $\Delta l_{PP} > 1.6$ mm)).

- Risk of expulsion was accompanied by the lowest value of electrode force and the higher value of welding current (**Table 8e**, parameter field 7).

The crucial aspect which remained was the failure to satisfy the principal criterion, i.e. the obtainment of the full weld nugget having a diameter of 1.5 mm.

The analysis of the FEM-based calculation results, presented in **Figure 5**, is as follows:

- In relation to the PFS, a welding current of 8.0 kA and a force of 1.0 kN, **Figure 5** presents the distribution of temperature within the entire range of temperature subjected to analysis, i.e. from ambient temperature to the melting point (liquidus) (**Figure 5a**). In such an approach, within the range of temperature, the melting of the material did not take place, and the weld nugget diameter calculated by the SOPRPAS software program amounted to a mere 0.2 mm. **Figure 5b** presents the distribution of temperature within the range of *solidus* (577°C) to *liquidus* (638°C). In the above-presented approach, within the entire range of welding time, it was impossible to obtain the melting of the material. As a result, the solid-state joint was formed within the entire area of contact.

- In relation to a higher current of 10.0 kA (F = 1.0 kN) and the PFS, energy supplied to the weld was higher. However, the plasticisation of the welding area combined with the exertion of constant and excessively high (electrode) force led to the situation where the material was melted and pushed outside. This, in turn, resulted in the increasingly large area of contact between the elements subjected to welding (bars), leading to the abrupt decrease in current density and, consequently, the immediate cooling of the weld material. Although it was possible to observe the melting of the material, the process was extremely short (2 ms) **Figure 5c2**. Precisely after two milliseconds, the temperature in the entire welding area decreased below the melting point (**Figure 5c3**).

- In relation to the lowest analysed current value amounting to 8.0 kA (**Figure 5d**) and the EFS, because of a different manner of electrode force control, it was easily possible to observe the welding of the material (subjected to welding) and the formation of the full weld nugget from the very beginning of the flow of welding current. In terms of the case under analysis, i.e. the welding of aluminium bars (Al 5182), the shutdown of current resulted in the immediate (within 1 ms) lowering of temperature below the melting point (**Figure 5d5–d6**). The foregoing indicated the intense discharge of heat from the welding area and, consequently, demanded process control-related parameters, i.e. welding current and electrode force. It should be noted that in relation to a current of 8.0 kA and the PFS, the joint formed within the entire area of contact (between the elements being welded) was in the solid state and no visible melting of the material had taken place (**Figure 5a**).

6.2 Experimental tests

In relation to the EFS and variants EE1 and EE2 from **Table 7**, it was possible to obtain the melting of the material within the entire area of the weld. Importantly, the melting of the material took place in the central (most favourable) part of the welded joint. The obtained weld nugget diameter exceeded the previously assumed value amounting to 1.5 mm (**Figure 8b1–b2**).

6.3 Comparison of results

The comparative metallographic test results concerning the PFS and EFS are presented in **Figure 8**. In relation to the PFS (**Figure 8a1–a2**), it was possible to observe the formation of the ring-shaped weld nearly within the entire range of technological cycle parameters (**Figures 6** and **7**). In terms of the EFS, the material subjected to welding was melted in the central part of the joint, and the weld nugget "grew" from inside towards outside.

7. Optimisation of the projection welding process illustrated with an example of the crosswise projection welding of bars

Based on the FEM calculation and experimental test results, the optimisation of the crosswise projection welding of (aluminium) bars could be characterised as presented below. The process of optimisation was performed on the basis of characteristic courses/waveforms of related parameters (electrode force, momentary power, electrode displacement and the weld nugget diameter) in relation to the two (i.e. pneumatic and electromechanical) electrode force systems (**Figure 9**).

To present the issue in a more convenient manner, the comparison was based on the same value of welding current, i.e. 8.0 kA. It should be emphasised that in relation to the PFS, the aforesaid value was insufficient to obtain a proper joint. The melting of the material was nearly invisible (**Figure 5b**). In turn, as regards the EFS, it was possible to obtain the full weld nugget having the previously assumed diameter exceeding a minimum of 1.5 mm (**Figure 5d**).

Curves 1 and 3 in **Figure 9** refer to the PFS, whereas curves nos. 2 and 4 are related to the EFS. Curves 3 and 4 present the welding current waveform in relation to the PFS and EFS, respectively.

There was a strict correlation between the characteristic process parameters, where the change of one of them immediately led to changes in the remaining parameters. To explain the existing correlations, it was necessary to divide the analysis of the process into stages.

The PFS-related process could be described as follows. After adjusting the preset constant electrode force (**Figure 9a**, curve 1) as well as the specific value of welding current and the time of current flow (**Figure 9a**, curve 3), during the first stage subjected to analysis (K1), specific welding energy was generated (**Figure 9b**, curve 1). The waveform of the welding power (stage K2) had a direct effect (ultimately) on the specific displacement of the electrodes (**Figure 9d**, curve 1). At the subsequent stage (K3), the effect of the above-named factors led to the obtainment of the weld nugget characterised by a specific shape and the diameter of a mere 0.2 mm (**Table 5**, variant P4; **Figure 9c**, curve 1).

As regards the use of the PFS, the value of welding current amounting to 8.0 kA was overly low, only enabling the plasticisation of the material and resulting in an excessive increase in the area of contact between the elements subjected to welding.

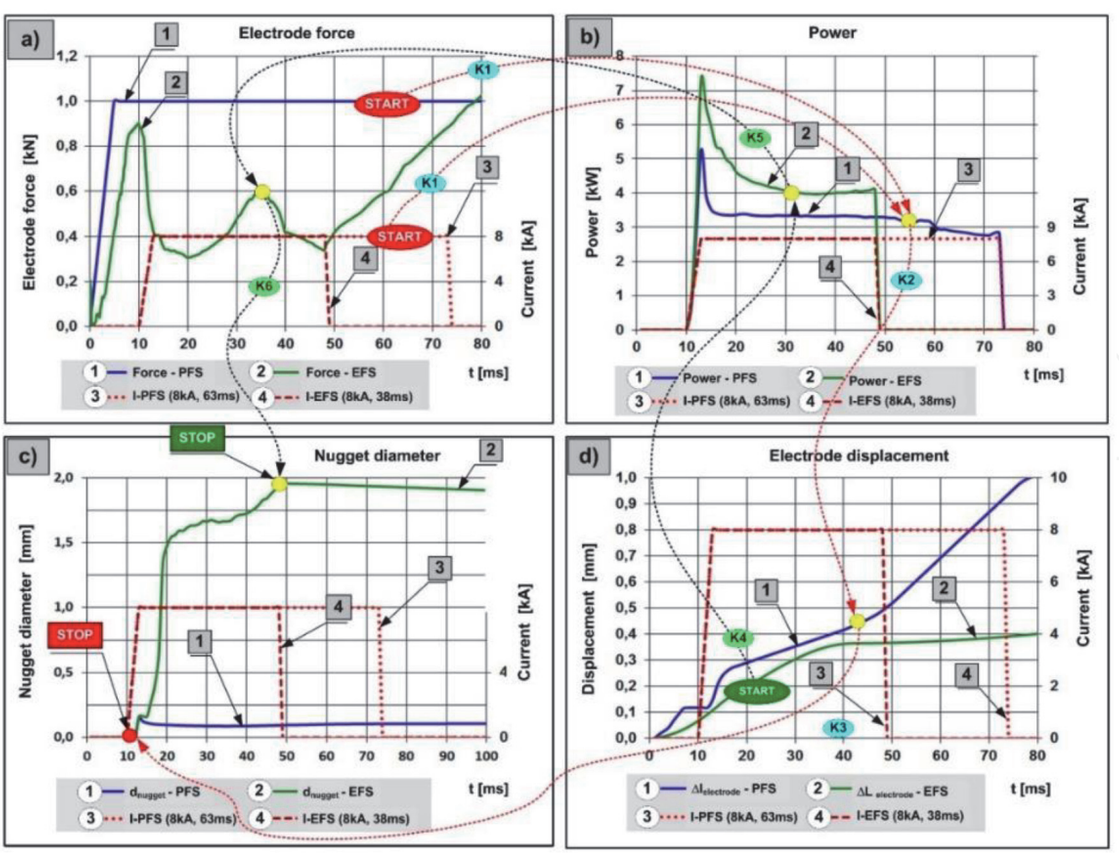

Figure 9.
FEM calculation results: (a) electrode force, (b) momentary power, (c) weld nugget diameter, (d) displacement of electrodes (bar penetration depth): —Curves 1 and 3, PFS (variant P1, I = 8.0 kA, F = 1.0 kN); —Curves 2 and 4, EFS (variant E1, I = 8.0 kA, force exerted by the servomotor).

The foregoing led to a decrease in current density and, consequently, precluded the melting of the material subjected to welding. The material in the contact area was only heated and plasticised, whereas the maximum welding time amounting to 63 ms was exceeded.

The starting point for the optimisation of the crosswise projection welding of bars involved a *proper* change in the course of the displacement of electrodes (bar penetration depth) (**Figure 9d**, curve 2) resulting from the use of the EFS and the application of an appropriate algorithm enabling the control of the electrodes [9]. The essence of the new method of control, i.e. a change in the course of the displacement of electrodes, consisted in the direct control of the aforesaid parameters, particularly during the flow of welding current. The new method of control involved the exertion of lower electrode force at the beginning of current flow and a decrease (slowing down) in the rate of displacement (of electrodes) aimed to obtain, at the subsequent stage (K4), the more favourable distribution of power density as well as to generate higher welding power (**Figure 9b**, curve 2) in comparison with those accompanying the use of the PFS [10]. The slowed down displacement of the electrodes combined with constant welding current led to an increase in resistance in the contact area between the elements (materials) subjected to welding and, consequently, an increase in welding power.

At the subsequent stage (K5), the above-presented method of control translated into the more favourable course of electrode force (**Figure 9a**, curve 2). The obtained values of electrode force were lower than those accompanying the use of the PFS. It should be noted that electrode force directly affected the value of resistance in the contact area (particularly in the *welded bar-welded bar* configuration), which, in turn, led to the proper space distribution of welding power and energy. As a result, the area of contact between the elements subjected to welding was smaller, the resistance in the aforesaid contact area was higher, and the distribution of temperature in the welding area was more favourable. All of the above-presented factors made it possible (at the final stage (K6)) to obtain the full wed nugget having the nominal diameter exceeding 1.5 mm (**Figure 9c**, curve 2). The aforesaid favourable outcome resulted from the more favourable distribution of temperature in the welding area, ultimately leading to the melting of the material and the formation of the weld nugget having the appropriately longer diameter.

The summary of the above-presented analysis concerning a welding current of 8.0 kA identified as overly low to obtain a proper joint using the PFS should contain a statement saying that the use of the EFS and the application of the appropriate control of electrode force and/or displacement (after satisfying the remaining requirements (quality-related criteria)) made it possible to significantly improve the welding process and obtain the full weld nugget having the diameter of a previously assumed length (> 1.5 mm).

8. Summary

The adjustment of the most favourable parameters in the crosswise projection welding of bars performed using the PFS is extremely difficult, if not impossible, particularly as regards soft materials such as aluminium alloys. Electrode force is unfavourably excessively high in relation to necessarily short welding time (bars Al 5182 – 40–60 ms) and high welding current. Such conditions are mutually exclusive and constitute a significant obstacle when adjusting welding parameters. The primary limitation is the dynamics of the electrode force system, i.e. the impossibility of quickly controlling electrode force in short time, particularly during the flow of current.

A characteristic of the PFS is the fact that the preset parameter is (electrode) force and the resultant parameter is the displacement (of electrodes), not controlled in any way.

The improvement of the welding process (extension of the window of parameters) requires the use of the EFS. In the operating mode involving the displacement of electrodes, it is possible to set a more convenient trajectory of electrode movement, enabling the obtainment of the more favourable distribution of current density and the more favourable space distribution of welding power. This, in turns, translates into the generation of higher energy in the central area of the joint and, as result, the generation of higher temperature in the aforesaid area and, consequently, the obtainment of the full weld nugget having larger dimensions that those obtainable using the PFS.

The use of the EFS makes it possible to control the displacement of the electrodes during the flow of current, reach the final, previously assumed, position of the electrodes and exert lower final pressure (force) by the electrodes.

The FEM calculation results indicate the possibility of successful welding using even lower welding current than that used in the experimental verification (8.0 kA).

Acknowledgements

This work was supported by the Polish National Centre for Research and Development (NCBR) under project no. TANGO1/267374/NCBR/2015 and co-funded by Łukasiewicz – Instytut Spawalnictwa, Poland.

Acronyms

PFS	pneumatic (electrode) force system
EFS	electromechanical (electrode) force system
t_{PP}/CFT	(welding) current flow time
upslope	time of current upslope from the initial to the final value of the cycle range
MFWC	most favourable welding conditions
EFST	electrode force stabilisation time
$\Delta L_{PP\ max} - \Delta L_{PB\ max}$	maximum displacement of electrodes (penetration of bars)
$T_{e\text{-}m\ max}$	maximum temperature in the *electrode – welded material* contact area

Glossary

Weld nugget is a part of the spot, projection or seam weld molten during the welding process [20].

Expulsion signifies the expulsion (during welding) of the molten metal from the area of contact between elements subjected to welding or from the area of contact between the electrode and a given element subjected to welding [21].

Welding area in spot or projection welding (e.g. of sheets with an embossed projection) is the area including the weld nugget, heat affected zone (HAZ) as well as the area of contact between the electrode and the material subjected to welding along with adjacent areas.

IntechOpen

Author details

Zygmunt Mikno
Research Network ŁUKASIEWICZ, Institute of Welding, Gliwice, Poland

*Address all correspondence to: zygmunt.mikno@is.gliwice.pl

References

[1] Zhang H, Senkara J. Resistance Welding Fundamentals and Applications. USA: CRC Press, Taylor & Francis Group; 2011

[2] Zhang X, Chen G, Zhang Y, Lai H. Improvement of resistance spot weldability for dual-phase (DP600) steels using servo gun. Journal of Materials Processing Technology. 2009; **209**(5):2671-2675

[3] Slavick SA. Using servo guns for automated resistance welding. Welding Journal. 1999;**78**(7):29-32

[4] Tang H, Hou W, Hu S. Forging force in resistance spot welding. Proceedings of the Institution of Mechanical Engineers, Part B: Journal of Engineering Manufacture. 2002;**216**(7):957-968. DOI: 10.1243/09544050260174166

[5] Gould JE. Joining aluminum sheet in the automotive industry—A 30 year history. Welding Journal (Welding Research). 2012;**91**:23-34

[6] Zhang XQ, Chen GL, Zhang YS. On-line evaluation of electrode wear by servo gun. International Journal of Advanced Manufacturing Technology. 2008;**36**:681-688

[7] Mikno Z. Projection welding with pneumatic and servomechanical electrode operating force systems. Welding Journal (Welding Research). 2016;**95**:286-299

[8] Mikno Z, Stepien M, Grzesik B. Optimization of resistance welding by using an electric servo actuator. Welding in the World. 2017. DOI: 10.1007/s40194-017-0437-x

[9] Mikno Z, Bartnik Z, Ambroziak A, Pietras A. Method for projection resistance welding of steel plates with embossed projections. In: Patent P. 220870. Polish Patent Office; 2012

[10] Mikno Z, Grzesik G, Stepien M. A manner of resistance projection welding in configuration of the cross, mainly for aluminum wires. In: Patent P. 228089. Polish Patent Office; 2015

[11] Mikno Z. Cross-wire projection welding of aluminium alloys in relation to pneumatic and electromechanical electrode force systems. International Journal of Advanced Manufacturing Technology. 2019;**102**:4167-4178. DOI: 10.1007/s00170-019-03443-5

[12] Mikno Z. Projection welding of nuts involving the use of electromechanical and pneumatic electrode force. International Journal of Advanced Manufacturing Technology. 2018:1-21. DOI: 10.1007/s00170-018-2525-5

[13] Mikno Z, Gradkowski M. System pneumatycznego docisku w zgrzewaniu rezystancyjnym. Biuletyn Instytutu Spawalnictwa. 2019;**5**(2019):13-18

[14] The database of the material and electrode parameters: model 3D Version 4.0x64 of the Swantec Inc., SORPAS Software. Available from: http://swantec.com/

[15] User Manual SORPAS® 3D Version 4.0 x64, SWANTEC Software and Eng. ApS; 2015

[16] Projection welding, Part 2 Chapter 2. Welding Processes. AWS Welding Handbook, Vol. 3. 9th ed.

[17] Gould JE. Projection welding. In: ASM Handbook. Vol. 6: Welding, Brazing, and Soldering. USA: ASM International; 1993. pp. 230-237

[18] Papkala H. Resistance Welding of Metals. Krosno: Publishing House KaBe; 2003

[19] Statistica 12. Available from: www.statsoft.pl

[20] Szczeciński Z et al. wytyczne nr W-90/IS-45, SPAWALNICZY SŁOWNIK TERMINOLOGICZNY. 1990

[21] Wyroby płaskie walcowane na gorąco ze stali o podwyższonej granicy plastyczności do obróbki plastycznej na zimno, Część 2: Warunki techniczne dostawy wyrobów walcowanych termomechanicznie. PN-EN 10149-2: 2014-02